



RESEARCH LETTER

10.1029/2021GL096519

Assessing Volcanic Controls on Miocene Climate Change

Jack Longman¹ , Benjamin J. W. Mills² , Yannick Donnadieu³, and Yves Godd ris⁴

Key Points:

- A new climate-biogeochemical model allows investigation of drivers of climate change in the Miocene
- Columbia River Basalt Group (CRBG) degassing is sufficient to have caused the Mid Miocene Climatic Optimum (MMCO)
- Weathering of CRBG insufficient to drive cooling after the MMCO. This may be linked to evaporite deposition and changes to marine chemistry

Supporting Information:

Supporting Information may be found in the online version of this article.

Correspondence to:

J. Longman and B. J. W. Mills,
jack.longman@uni-oldenburg.de;
B.Mills@leeds.ac.uk

Citation:

Longman, J., Mills, B. J. W., Donnadieu, Y., & Godd ris, Y. (2022). Assessing volcanic controls on Miocene climate change. *Geophysical Research Letters*, 49, e2021GL096519. <https://doi.org/10.1029/2021GL096519>

Received 19 OCT 2021

Accepted 21 DEC 2021

Author Contributions:

Conceptualization: Jack Longman, Benjamin J. W. Mills
Formal analysis: Jack Longman, Benjamin J. W. Mills
Investigation: Jack Longman, Benjamin J. W. Mills
Methodology: Jack Longman, Benjamin J. W. Mills, Yannick Donnadieu, Yves Godd ris
Resources: Jack Longman, Benjamin J. W. Mills, Yannick Donnadieu, Yves Godd ris
Software: Benjamin J. W. Mills, Yannick Donnadieu, Yves Godd ris
Validation: Jack Longman, Benjamin J. W. Mills

  2022. The Authors.

This is an open access article under the terms of the [Creative Commons Attribution License](https://creativecommons.org/licenses/by/4.0/), which permits use, distribution and reproduction in any medium, provided the original work is properly cited.

¹Marine Isotope Geochemistry, Institute for Chemistry and Biology of the Marine Environment (ICBM), University of Oldenburg, Oldenburg, Germany, ²School of Earth and Environment, University of Leeds, Leeds, UK, ³CNRS, IRD, INRA, CEREGE, Aix Marseille University, Coll ge de France, Aix-en-Provence, France, ⁴G osciences Environnement Toulouse, CNRS-Universit  de Toulouse III, Toulouse, France

Abstract The Miocene period saw substantially warmer Earth surface temperatures than today, particularly during a period of global warming called the Mid Miocene Climatic Optimum (MMCO; ~17–15 Ma). However, the long-term drivers of Miocene climate remain poorly understood. By using a new continuous climate-biogeochemical model (SCION), we can investigate the interaction between volcanism, climate and biogeochemical cycles through the Miocene. We identify high tectonic CO₂ degassing rates and further emissions associated with the emplacement of the Columbia River Basalt Group as the primary driver of the background warmth and the MMCO respectively. We also find that enhanced weathering of the basaltic terrane and input of explosive volcanic ash to the oceans are not sufficient to drive the immediate cooling following the MMCO and suggest that another mechanism, perhaps the change in ocean chemistry due to massive evaporite deposition, was responsible.

Plain Language Summary The Miocene period was much warmer than today, with the Mid Miocene Climatic Optimum (MMCO, roughly 17–15 million years ago) especially warm. Due to the high surface temperatures, comparisons to projected climatic conditions as a result of anthropogenic climate change have been drawn. However, the drivers of climate during the Miocene are not well understood. By using a new type of climate model, we investigate the impact volcanic eruptions had on the period, and link the extreme warmth of the MMCO with greenhouse gas release from the eruption of the Columbia River Basalts Group (CRBG). We find weathering of the CRBG does not explain the cooling at the end of the MMCO, and so discuss other potential explanations such as evaporite deposition.

1. Introduction

Miocene climate was generally warm, and the Mid Miocene Climatic Optimum (MMCO; ~17–15 Ma) was associated with a global average surface temperature around 5 C warmer than the pre-industrial (Burls et al., 2021; Goldner et al., 2014; Zachos et al., 2008). This resulted from a stronger greenhouse effect, with atmospheric CO₂ levels between 600 and 800 ppm (Rae et al., 2021). Projections of anthropogenic climate change predict that atmospheric CO₂ (pCO₂) will reach levels unseen since the MMCO (c. 600 ppm) by 2100 under ‘business as usual’ conditions (IPCC, 2014; Rae et al., 2021). The fact that Earth’s continental configuration was similar to modern-day, and that biota were close to modern (Steinthorsdottir et al., 2020), means the MMCO may be a good proxy for investigating future climatic change on Earth.

A warmer Miocene world is likely the result of higher rates of CO₂ input from arcs and rifts (Brune et al., 2017; Domeier & Torsvik, 2019; Merdith et al., 2019), combined with a less ‘weatherable’ continental surface (Caves Rugenstein et al., 2019; Raymo & Ruddiman, 1992), while the MMCO onset has been linked to the emplacement of the Columbia River Basalt Group (CRBG) in the northwestern United States (Barry et al., 2013; Reidel, 2015). The CRBG represents the effusive phase of a Large Igneous Province (LIP) which erupted between 17 and 6 Ma (Barry et al., 2013; Kasbohm et al., 2021; Kasbohm & Schoene, 2018). Recent research indicates ~95% of the CRBG was emplaced in a 750 kyr period from 16.7 Ma onwards (Kasbohm & Schoene, 2018), supporting the theory that volcanic greenhouse gas release may have led to the MMCO (Armstrong McKay et al., 2014; Babila & Foster, 2021).

The Mid-Miocene Climate Transition (MMCT) which follows the MMCO is less well understood, with numerous mechanisms potentially having played a role in the rapid cooling at ~13.9 Ma (Scotese et al., 2021; Westerhold et al., 2020). Research suggests that the MMCT is linked primarily to changes in ocean circulation,

Writing – original draft: Jack Longman, Benjamin J. W. Mills
Writing – review & editing: Jack Longman, Benjamin J. W. Mills, Yannick Donnadieu, Yves Godd ris

growth of Antarctic ice sheets (Levy et al., 2016) and $p\text{CO}_2$ decrease (Rae et al., 2021). High rates of organic carbon (C_{org}) burial during the MMCO are more likely a response to the warming and sea level rise rather than a factor in the subsequent cooling episode (Sosdian et al., 2020). Another explanation is the deposition of calcium sulphate evaporites, a process which increases ocean alkalinity and CO_2 uptake (Shields & Mills, 2021). This is supported by evidence for evaporite deposition across the Mediterranean during the Mid-Miocene (De Leeuw et al., 2010). One unexplored possibility is that volcanic eruptions themselves drove the cooling at the end of the MMCO. It is known basaltic terranes, such as the CRBG, are highly erodible and reactive, thus may increase the global rate of silicate weathering and CO_2 draw-down (Dessert et al., 2001, 2003). These terranes may also supply large amounts of nutrients to the oceans, where in the right conditions they stimulate productivity and sequester carbon via the biological pump (Dessert et al., 2003; Li et al., 2016). Furthermore, explosive volcanic eruptions, and deposition of volcanic ash in the oceans, are known to lead to enhanced drawdown and burial of marine C_{org} (Longman et al., 2019; Longman, Gernon, et al., 2021), potentially providing a separate sink for CO_2 .

In this study, we use the new SCION (Spatial Continuous Integration) Earth Evolution model (Mills et al., 2021) to investigate changes to the global carbon and nutrient cycles throughout the Miocene, with a particular focus on the MMCO and MMCT. SCION uses a 3-dimensional interpolation scheme to link physical climate model outputs (from the Fast Ocean Atmosphere Model – FOAM; Jacob, 1997) to long-term biogeochemical cycles. The model allows the investigation of changes to surface processes like silicate weathering in 2D over geological time under a realistic steady-state climate dynamically linked to the model carbon cycle (Mills et al., 2021). SCION is a ‘forwards’ model which makes predictions for climate and global elemental cycles using only tectonic and evolutionary boundary conditions, and relies on a large number of General Circulation Model (GCM) runs performed at discrete points in geological time and for a range of CO_2 levels (Donnadieu et al., 2006; Godd ris et al., 2014). Advances in modeling have been matched by recent advances in compilations of palaeo-proxy data (Rae et al., 2021; Scotese et al., 2021; Westerhold et al., 2020), and so comparisons between the two approaches should be possible at levels of accuracy previously unobtainable, helping us to assess the model predictions.

2. Materials and Methods

2.1. Model Setup and Scenarios

We use the SCION model version 1.1 for this work, which contains an important update to the first model version (1.0: Mills et al., 2021). In the original model, the Cenozoic climate was represented by GCM runs at 52, 30 and 0 Ma. In this version, we add GCM runs for 15 Ma, which were part of the set used by Godd ris et al. (2014) but had not been converted for the SCION framework due to the whole-Phanerozoic focus of the first SCION paper and some minor issues in scaling the digital elevation model to the same resolution as the climate outputs, which have now been resolved. The model is run forwards in time for the whole Phanerozoic, as in Mills et al. (2021), but we only show the Oligocene-to-present estimates here. We concentrate on the model predictions for atmospheric CO_2 , global average surface temperature and whole-ocean $\delta^{13}\text{C}$ of DIC, and use 1000-member ensembles to test the variation in key parameters as in Mills et al. (2021). An extended description of the model may be found in Text S1 of Supporting Information S1. The full model flux data are included in Figure S1 of Supporting Information S1 and the model code can be downloaded at <https://github.com/bjwmills/SCION>.

2.2. Model Scenarios

Figure 1 shows the evolving continental configuration, including the location of the CRBG, alongside the modified chemical inputs assumed throughout the model runs. The baseline model assumes a decreasing rate of CO_2 input throughout the last 30 million years, based on the declining material subduction rate (Domeier & Torsvik, 2019) and the reduction in the extent of continental arcs and rifts (Brune et al., 2017; Mills et al., 2017). The uncertainty range is described in Mills et al. (2021) and represents the boundaries of the estimates based on arc length alone versus those based on material subduction flux alone.

To estimate CRBG degassing flux (orange in Figure 1d) we use the timeframe of 16.7 to 15.9 Ma, and derive a maximum CO_2 flux estimate in a manner similar to Armstrong McKay et al. (2014). This method compares the size of the CRBG and that of the Siberian traps, probably the most well-studied LIP in terms of its ‘cryptic degassing’ budget – carbon degassed from the surrounding sediments rather than the basalt itself, which forms the major part of the CO_2 budget (perhaps 90%; Armstrong McKay et al., 2014; Svensen et al., 2009). A conservative

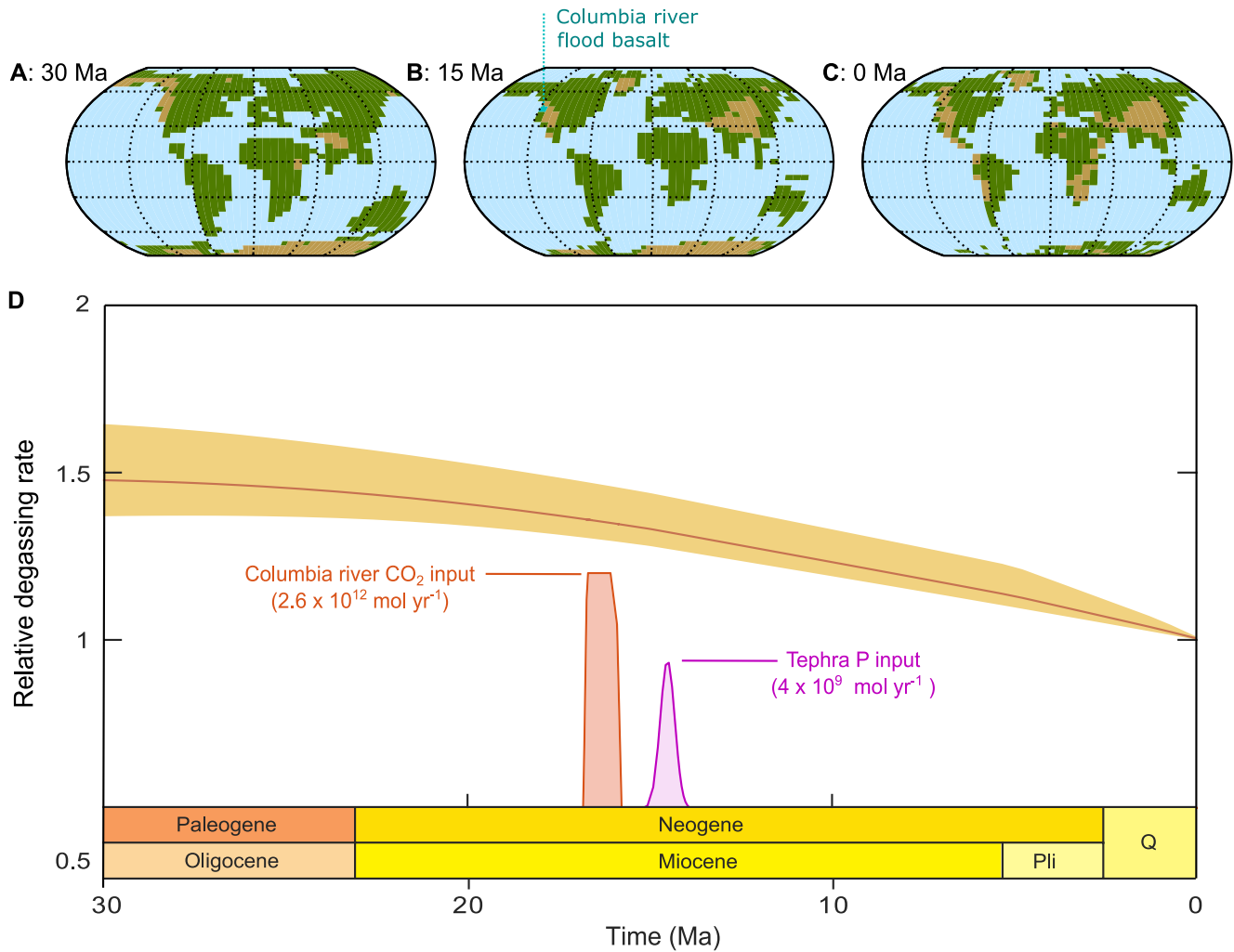


Figure 1. Summary of topographical change for the three GCM model runs used in this study: 30 Ma (a), 15 Ma (b) and 0 Ma (c). Green and brown grid cells indicate topography below and above 1 km respectively. Panel B shows the location of the Columbia River Basalt Group (CRBG). D displays the long-term CO₂ degassing rate (orange line) and the two proposed forcings tested by this work, the input of excess CO₂ from the emplacement of the CRBG, and phosphorous input to the oceans from the deposition of tephra in central Europe.

estimate places the Siberian traps volume at roughly $1 \times 10^6 \text{ km}^3$ (Ivanov et al., 2013), five times the volume of the CRBG ($2 \times 10^5 \text{ km}^3$; Reidel et al., 2013), meaning the contacted surface area of surrounding sediment was around three times that of the CRBG (assuming spherical shape). Thus, an assumed cryptic degassing flux of $7.2 \times 10^{12} \text{ mol C yr}^{-1}$ from the Siberian traps (Dal Corso et al., 2020; Svensen et al., 2009) would imply a flux of $2.38 \times 10^{12} \text{ mol C yr}^{-1}$ from the CRBG, for a total maximum possible CO₂ degassing of $2.64 \times 10^{12} \text{ mol yr}^{-1}$, assuming the CRBG was emplaced into relatively carbon-rich surroundings (Armstrong McKay et al., 2014).

We include the emplacement of the CRBG as a highly weatherable terrane covering the entire gridbox around latitude 47°N, 60°W (Figure 1b). The gridbox area is 280,000 km², similar to the estimated initial area of the CRBG (Ernst et al., 2021; Mills et al., 2014; Reidel et al., 2013). The CRBG is included in the land map for 15 Ma but not in the present-day simulation, assuming that its enhanced weathering effect has waned sufficiently (Vance et al., 2009). The weathering effects of the LIP are assumed to begin at 16.7 Ma and are linearly interpolated out of the land map between 15 and 0 Ma. We calculate the weathering effects in a similar manner to previous research (Goddéris et al., 2017; Lefebvre et al., 2013). Total present-day mafic rock area is around 6.8 million square kilometers (Mkm²), contributing ~35% of the silicate weathering flux (Dessert et al., 2003). The total weatherable land area which may contain silicates (i.e., ignoring carbonates and evaporites) is about 120 Mkm² (Hartmann et al., 2014). So, if mafic lithologies represent around ~5% of weatherable silicates, we determine

them to be ~ 7 times more weatherable than the homogeneous silicates which comprise the remainder of the model land surface. Thus, we multiply the silicate weathering flux for the CRBG gridcell by a factor 7. Sensitivity tests are detailed in Table S1 of Supporting Information S1.

To consider nutrient supply from the major silicic volcanic episodes in central Europe during the Mid-Miocene (Lukács et al., 2018), we use an ash depletion model adapted from Lee et al. (2018). This approach uses the GeoROC database to estimate the initial composition of erupted volcanic material, before comparing it to measured compositions of altered tephra to estimate the amount of phosphorous loss (Longman, Mills, et al., 2021). This is then used to estimate productivity increases associated with the input of P by including it as an additional P flux to the model ocean. There are two clear pulses of volcanic input at 14.36 and 14.88 Ma, associated with the eruption of the Harsany and Demjen tephtras (Lukács et al., 2018). To estimate the volume of these eruptions and the amount of P supplied, we use Monte Carlo simulations considering errors on a range of variables. For the two relevant tephtras, we estimate their volume as a proportion of the total 4,000 km³ erupted across the Mid Miocene, using their relative extent (compared to the total extent of all tephtras) as observed in outcrops (Lukács et al., 2018). For Monte Carlo simulations, we estimate error on these values to be 20%. We then convert these values to P supply using ash density, P content and P depletion factors (and associated errors) from Longman, Mills, et al. (2021). Finally we assume 90% of the erupted tephra was deposited in the ocean, based on paleogeographic reconstructions (Lukács et al., 2018). These formations were deposited in what was the Pannonian Sea, a back-arc basin which persisted in central Europe until the Pliocene Epoch (Balázs et al., 2016). All variables and their associated errors used in the Monte Carlo modeling may be found in Table S2 of Supporting Information S1. For simplicity we model these eruptions as a single Gaussian input curve which begins at the timing of the Harsany tephra and peaks at the timing of the Demjen tephra, as the model is not designed to represent timescales of less than 100 kyrs.

3. Results and Discussion

The SCION model baseline run (Figures 2a–2c; no LIP and no tephra) simulates the long-term temperature decline of the Miocene well, but overestimates CO₂ before ~ 10 Ma (Figure 2b). This is likely due to the low CO₂ climate sensitivity of the FOAM climate model (Donnadieu et al., 2006; Goddérís et al., 2014), meaning relatively high CO₂ levels are required to raise the surface temperature to a point of carbon cycle balance (Mills et al., 2021). Climate and carbon cycle balance at 15 Ma has previously been simulated in the GEOCLIM model using the same climate model runs that we use here (Lefebvre et al., 2013). The previous investigation used a present-day CO₂ degassing rate rather than an elevated rate of degassing, resulting in lower steady state CO₂ concentrations than the current model – ~ 500 ppm. Here, the increase over preindustrial levels was due partly to the positioning of weatherable basaltic terranes in arid areas, not considered in the present work. Returning to the SCION predictions, a clear mismatch between the baseline output and proxy data is visible during the MMCO (~ 17 –14 Ma) and the following MMCT (13.9–12 Ma) where the model does not capture temperature, CO₂ and the carbon isotope composition change associated with climatic variability (Figure 2).

The addition of degassing from the emplacement of the CRBG improves this mismatch considerably across the MMCO, especially regarding global temperature change (Figures 2d–2f). Previous modeling used a smaller CO₂ input, even when a cryptic element was considered, insufficient to force the MMCO in its entirety (Armstrong McKay et al., 2014). The difference here is that our calculations are based on new chronological constraints indicating the majority of CRBG emplacement in as little as 750 kyr (Kasbohm & Schoene, 2018), and our method of comparison to the Siberian traps considers the difference in contacted sediment surface area directly. The injection of CO₂ associated with this event is sufficient to drive the MMCO inception, and constraining the majority of CO₂ degassing to a short period after 16.7 Ma places the CRBG emplacement at the same time as the onset of the MMCO (Kasbohm & Schoene, 2018). Such a finding supports previous assertions of a causative link between Mid Miocene volcanism and climate change (Hodell & Woodruff, 1994; Kasbohm & Schoene, 2018; Kürschner et al., 2008; Steinthorsdóttir et al., 2021).

The model estimate of global temperature increase at the MMCO onset is $\sim 1^\circ\text{C}$, lower than some proxy reconstructions (e.g., 2.3°C rise; Scotese et al., 2021). However, this is well within proxy reconstruction variability and is also somewhat affected by a low climate sensitivity in FOAM compared to more complex modern climate models (e.g., Zhu et al., 2019). It is possible that other greenhouse gases were also released as part of the CRBG

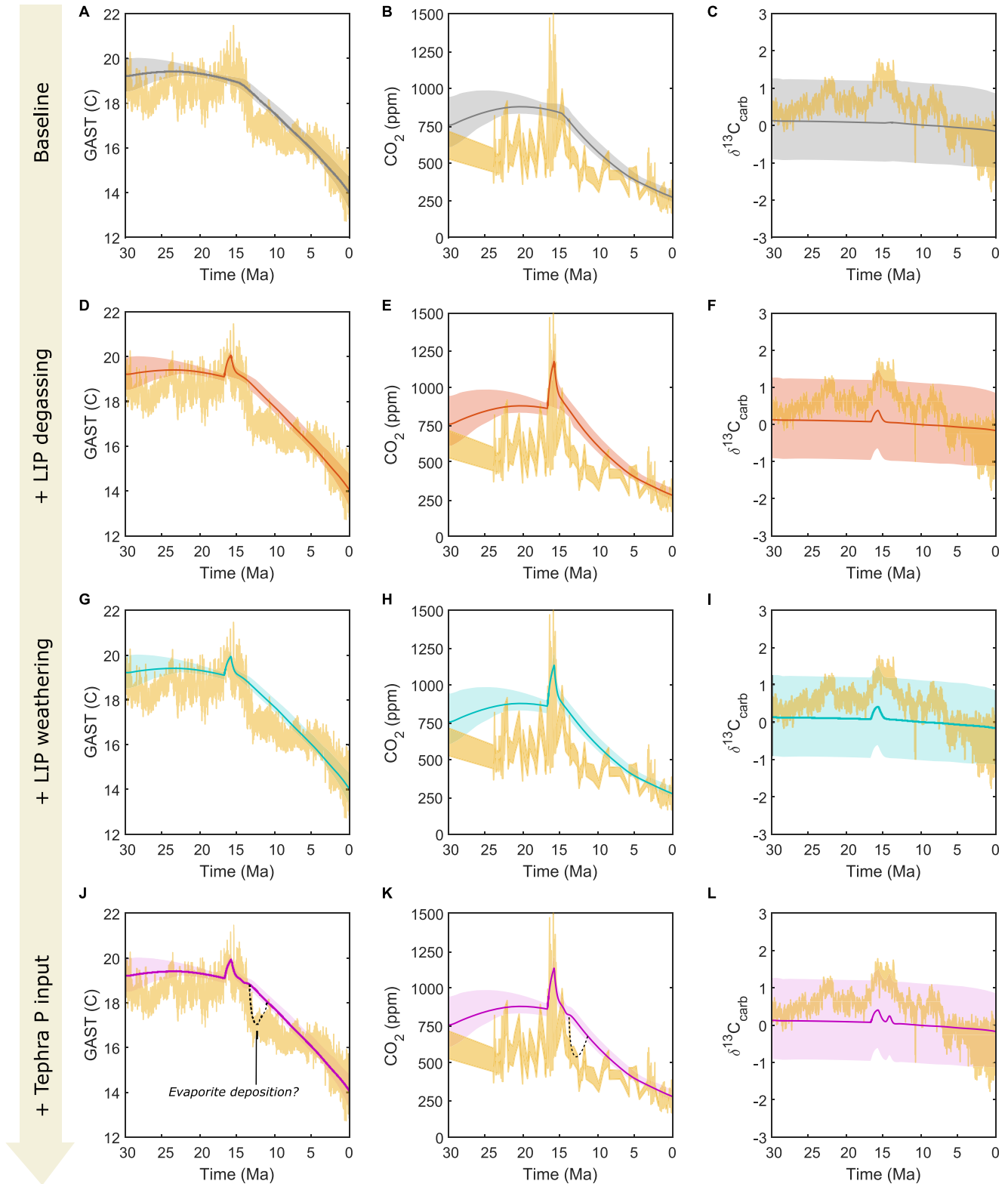


Figure 2. Model outputs of global average surface temperature (GAST), atmospheric CO₂ and carbonate δ¹³C, comparing various SCION runs through the Miocene. (a–c) display the baseline SCION run, with no additional forcings. (d–f) show the baseline with additional LIP CO₂ degassing. (g–i) show baseline with additional LIP CO₂ degassing and basaltic terrane weathering. (j–l) show baseline with additional LIP CO₂ degassing, basaltic terrane weathering and phosphorous supply from tephra input. The surface temperature approximation is calculated from the oxygen isotope data set of Westerhold et al. (2020), under the temperature conversion of Hansen et al. (2013). CO₂ proxy data is from boron isotope measurements (indicative of pH) from Rae et al. (2021). Carbon isotope data is from Westerhold et al. (2020).

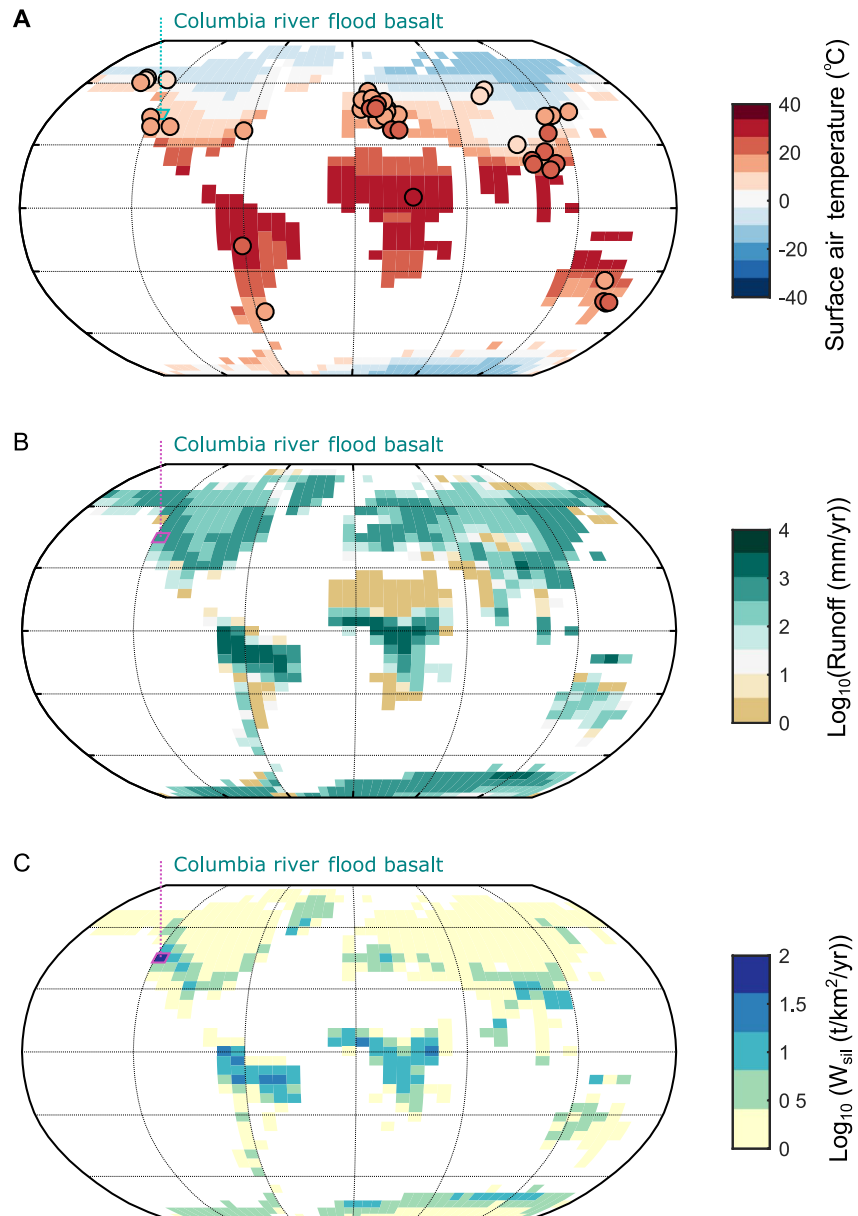


Figure 3. Gridded map outputs for the complete SCION model scenario shown in Figures 2j–2l at 15 Ma. Displayed here are surface air temperature (a), continental runoff (b) and silicate weathering rates (c). Panel A includes a comparison of model surface air temperature at 15 Ma with proxy reconstructions of mean annual temperature (filled circles; Goldner et al., 2014), with map colors the same as the individual proxy reconstructions. All panels show the location of the Columbia River basalt using a dashed line.

emplacement, with evidence for hydrothermal alteration of organic-rich sediments and associated CH_4 release (Bindeman et al., 2020), potentially enhancing the greenhouse effect. Comparison of the model output with reconstructions of CO_2 further supports an assertion of CRBG degassing as a primary driver of Mid Miocene climatic change (Figure 2), with simulated CO_2 of $\sim 1,200$ ppm at the MMCO peak in line with previous reconstructions (Rae et al., 2021), but above a number of previous estimates (e.g., Steinthorsdottir et al., 2020, 2021).

The spatial pattern of modeled surface air temperatures at 15 Ma (Figure 3a) shows general agreement with a data set of MMCO proxy reconstructions of temperature (Goldner et al., 2014). The largest offsets between model and proxy data are in polar regions, where the model simulates anomalously low temperatures (Figure 3a). This is a common issue when modeling warm periods of the Earth history such as the Eocene and the Pliocene (Haywood

et al., 2020; Huber & Caballero, 2011), and it remains a challenge to successfully model the Miocene polar regions with fully coupled ocean-atmosphere models (Burls et al., 2021).

We assume a value of zero for the $\delta^{13}\text{C}$ composition of the CRBG-degassed CO_2 . While mantle-derived carbon would be expected to have a negative fractionation compared to the PDB standard, most of the degassed carbon is assumed to have come from sediments with varied fractionations. The SCION model has an average sediment $\delta^{13}\text{C}$ value of zero, used here in the absence of more detailed constraints. It is possible that Miocene volcanic carbon contained more positive $\delta^{13}\text{C}$ than usual, although there is little experimental evidence of such $\delta^{13}\text{C}$ values in mantle carbon (Deines, 2002). Under the current scenario, the model produces a small positive $\delta^{13}\text{C}$ excursion during the CRBG degassing due to elevated temperature, weathering, and productivity. This suggests the hypothesis of Sosdian et al. (2020) may be correct; high atmospheric CO_2 across the MMCO led to a positive shift in the fractionation factor associated with photosynthesis, offsetting any negative mantle $\delta^{13}\text{C}$ emissions (Armstrong McKay et al., 2014; Sosdian et al., 2020). This additional factor is not considered in the model, but the error window on $\delta^{13}\text{C}$ shown encompasses likely changes due to photosynthetic fractionation (Mills et al., 2021).

By also modeling enhanced silicate weathering from the CRBG, we consider the impact of LIP emplacement holistically across the Mid Miocene (Figures 2g–2i). Basaltic terranes such as the CRBG are highly erodible and the products which enter the oceans contain abundant silicate cations and are nutrient-rich (Dessert et al., 2001, 2003; Gaillardet et al., 1999; Hartmann et al., 2009; Li et al., 2016). As such, it has been suggested that as well as increasing silicate weathering rates, these nutrients may enhance productivity, and raise the levels of marine organic carbon (C_{org}) burial, a process which removes CO_2 from the ocean-atmosphere system and leads to cooling on long timescales (Bernier et al., 1983; Li et al., 2016; Li & Elderfield, 2013).

The inclusion of CRBG weathering in the SCION model has little impact on the model results (Figures 2g–2i). This is because although the terrain is assumed to contribute seven times more silicate weathering (and P delivery) than the rest of the model homogeneous lithology, it still only represents a small fraction of the land surface and is emplaced in an area of relatively low temperature in the high latitudes. The position of the CRBG in the model is in an area where temperature is well-predicted (Figure 3a), and runoff rates are reasonably high (Figure 3b). Accordingly, the weathering rate of the CRBG is estimated to be more than two times higher than any local gridcell. Despite this clear contribution to high-latitude weathering, its overall weathering contribution is similar to a single equatorial gridcell.

It has been proposed that MMCO length was extended by a delayed silicate weathering feedback (Babila & Foster, 2021), but our model results suggest the warm interval length is consistent with the single injection of mantle CO_2 , with no clear requirement for a delay in the onset of CRBG weathering to reproduce proxy data (Figure 2). Additionally, the scale of sequestration associated with silicate weathering of the CRBG does not appear to be sufficient to drive the transition to cooler climate after ~ 13.9 Ma, the end of the MMCO (Steinthorsdottir et al., 2020), with proxy evidence suggesting a much more rapid shift to cooler temperatures than the SCION reconstruction (Figure 2g).

We now consider other potential controls on Miocene cooling. In central Europe, extremely large tephra deposits ($\sim 4,000$ km³ tephra per eruption) are preserved (Lukács et al., 2018). Since these primarily erupted into the Paratethys Ocean, and as the alteration of tephra is known to release nutrients (Browning et al., 2015; Frogner et al., 2001; Jones & Gislason, 2008; Longman et al., 2019), we consider these as a potential source of bioavailable nutrients to the ocean system. Dates for these eruptions indicate two pulses, the first at 18.2–16.8 Ma, and the second between 14.9 and 14.4 Ma (Lukács et al., 2018), with evidence of ashfall from southern Germany (Arp et al., 2021) to western Russia (Danišík et al., 2021) indicative of the scale of the events. Using a separate modeling approach (see Methods), we are able to estimate the scale of P supply from these eruptions (Figure 1). The input of additional P to the ocean plays very little role in global-scale climate change in our model (Figures 2j–2l). This contrasts with a separate study, which linked the Ordovician glaciations to tephra-derived P supply (Longman, Mills, et al., 2021), indicating the volcanic episodes observed in central Europe across the mid-Miocene were not large enough to play a major role in global climate cycles – the P supply we calculate here is more than an order of magnitude smaller than the Ordovician events.

Another mechanism which may have enhanced the cooling feedback following the CRBG emplacement is the relatively high sea levels during the MMCO, a result of Antarctic ice shelf loss (Gasson et al., 2016; Lear et al., 2010; Steinthorsdottir et al., 2020). Higher sea levels would have flooded large areas of shallow continents, and resulted

in larger areas of continental shelves (Sosdian et al., 2020), locations known to be centers of C_{org} burial (Bianchi et al., 2018; Burdige, 2007). It is possible high CO_2 atmospheres as a result of volcanism during the MMCO provided a source of carbon to the upper ocean, with nutrients additionally supplied by weathering of the CRBG (Sosdian et al., 2020). Easily available nutrients, high atmospheric CO_2 , and high temperatures combined with the large extent of continental shelves, likely resulted in the deposition of large areas of C_{org} -rich sediments in the circum-Pacific area (e.g., the Monterey formation; Flower & Kennett, 1993; Pisciotto & Garrison, 1981). There is evidence to suggest the high C_{org} contents are not related to exceptionally high productivity, rather near-perfect conditions for preservation (Föllmi et al., 2005; Laurent et al., 2015). Whatever the exact mechanism, the timing of this event (~16–14 Ma; Sosdian et al., 2020) indicates it cannot have played a role in the MMCT, but was rather a feature of the warm temperatures in the aftermath of the CRBG emplacement. Our modeling supports this assertion, with global C_{org} burial rates increasing by 10% during the MMCO.

Another proposed cooling mechanism at the end of the MMCO is the closure of the Panama gateway (Montes et al., 2015), which led to the formation of the Atlantic Meridional Overturning Circulation (AMOC), which in the modern ocean acts as the single largest carbon sink in the Northern Hemisphere (Gruber et al., 2002). Research has suggested this occurred between 15 and 12 Ma, a period which could have implications for the end of the MMCO and the MMCT (Bacon et al., 2015; Montes et al., 2015). However, most evidence suggests ongoing throughflow between the Pacific and the Atlantic until the Pliocene (Karas et al., 2017; Lessios, 2015; O'Dea et al., 2016; Panitz et al., 2018).

The timing of the end of the MMCO also correlates well with evidence for intensification of physical weathering in the Himalaya Mountains linked to the onset of the winter monsoon (Ali et al., 2021; Bretschneider et al., 2021; Lee et al., 2020). This supports studies which proposed that enhanced weathering of the Himalayas led to Miocene cooling but were limited by temporal uncertainties (Allen & Armstrong, 2012; Tada et al., 2016). Such a process would have enhanced CO_2 drawdown, and may have led to cooling (Allen & Armstrong, 2012), but it is unlikely this process was sizable enough to have controlled the end MMCO cooling (Clift & Jonell, 2021). Earlier work using these FOAM simulations has shown that the South Asian Monsoon amplified silicate weathering rates at the present-day, relative to 15 Ma (Lefebvre et al., 2013), and this feature persists in the SCION model. More detailed testing of monsoonal effects on climate on the Myr scale would require a larger set of continental configuration and climate model runs.

Another potential cause for the rapid cooling observed at the MMCT is widespread evaporite deposition (Shields & Mills, 2021). Deposition of thick calcium sulphate evaporites depletes ocean calcium, impacting calcium carbonate precipitation and increasing marine alkalinity. This alkalinity increase leads to drawdown of CO_2 into the ocean on a million-year scale, before the silicate weathering feedback balances the alkalinity and calcium budget and restores equilibrium (Shields & Mills, 2021). It has been demonstrated that around 10^{19} mol of gypsum deposition would roughly halve oceanic Ca concentration, potentially driving ~1.5 degrees of cooling over 1 Myr (Shields & Mills, 2021). The mid-Miocene did indeed see widespread evaporite deposition, culminating in the Badenian Salinity Crisis at around 13.8 Ma and the deposition of evaporite facies across much of eastern Europe (De Leeuw et al., 2010; Peryt, 2006). The total weight of sulphate evaporites deposited is uncertain, but the estimated budget for the whole Miocene (including the later Messinian Salinity Crisis) is around 1.5×10^{19} mol (Hay et al., 2006), so is compatible with a large Langhian-Serravallian deposition contributing to the MMCT. The impact of evaporite disposition on climate cannot be explicitly modeled in SCION because it employs steady-state carbonate chemistry, but it is feasible that the disconnection between model and proxy data 15–13 Ma is linked to this process (Figures 2j and 2k).

4. Conclusions

Using a new coupled biogeochemical-climate model, we investigate the driving forces behind the climate of the Miocene. We demonstrate the emplacement of the Columbia River Basalt Group, and associated CO_2 degassing led to the warming of the Mid Miocene Climatic Optimum (MMCO; 17–15 Ma). The modeled response of the Earth system to the injection of magmatic CO_2 is very similar in magnitude and extent of the warming and CO_2 increase observed in proxy records from this time. The cooling following the MMCO cannot be easily explained by either weathering of the basalt group, or a greater phosphorus supply associated with large-scale volcanism. The abundant organic carbon deposition observed in Pacific facies across the MMCO (the Monterey event) is also

unlikely to have driven to the cooling, rather it appears this was a feature of high MMCO temperatures leading to greater productivity. We suggest the most likely cause of the rapid cooling period is the emplacement of giant evaporites in central-eastern Europe, which depleted the ocean calcium reservoir and raised ocean alkalinity.

Data Availability Statement

All data from the model runs is presented in the Supporting Information, and available for download at <https://doi.org/10.6084/m9.figshare.17306372>. The model code is available at <https://github.com/bjwmills/SCION> and permanently archived at <https://doi.org/10.5281/zenodo.5819102>.

Acknowledgments

The authors appreciate the comments and suggestions of two anonymous reviewers, who helped to improve the manuscript. Benjamin J. W. Mills was funded by the UK Natural Environment Research Council grant NE/S009663/1. Yannick Donnadiou acknowledges the support of the French Research Agency (ANR) project AMOR (2016-CE31-020). Open access funding enabled and organized by Projekt DEAL.

References

- Ali, S., Hathorne, E. C., & Frank, M. (2021). Persistent provenance of South Asian monsoon-induced silicate weathering over the past 27 million years. *Paleoceanography and Paleoclimatology*, *36*(3), e2020PA003909. <https://doi.org/10.1029/2020PA003909>
- Allen, M. B., & Armstrong, H. A. (2012). Reconciling the intertropical convergence zone, Himalayan/Tibetan tectonics, and the onset of the Asian monsoon system. *Journal of Asian Earth Sciences*, (Vol. 44, pp. 36–47). Pergamon. <https://doi.org/10.1016/j.jseas.2011.04.018>
- Armstrong McKay, D. I., Tyrrell, T., Wilson, P. A., & Foster, G. L. (2014). Estimating the impact of the cryptic degassing of large igneous provinces: A mid-Miocene case-study. *Earth and Planetary Science Letters*, *403*, 254–262. <https://doi.org/10.1016/j.epsl.2014.06.040>
- Arp, G., Dunkl, I., Jung, D., Karius, V., Lukács, R., Zeng, L., et al. (2021). A volcanic ash layer in the Nördlinger Ries impact structure (Miocene, Germany): Indication of crater fill geometry and origins of long-term crater floor sagging. *Journal of Geophysical Research: Planets*, *126*, e2020JE006764. <https://doi.org/10.1029/2020je006764>
- Babila, T. L., & Foster, G. L. (2021). *The Monterey event and the Paleocene-Eocene thermal maximum* (pp. 401–416). American Geophysical Union (AGU). <https://doi.org/10.1002/9781119507444.ch17>
- Bacon, C. D., Silvestro, D., Jaramillo, C., Smith, B. T., Chakrabarty, P., & Antonelli, A. (2015). Biological evidence supports an early and complex emergence of the Isthmus of Panama. *Proceedings of the National Academy of Sciences*, *112*(19), 6110–6115. <https://doi.org/10.1073/PNAS.1423853112>
- Balázs, A., Matenco, L., Magyar, I., Horváth, F., & Cloetingh, S. (2016). The link between tectonics and sedimentation in back-arc basins: New genetic constraints from the analysis of the Pannonian Basin. *Tectonics*, *35*(6), 1526–1559. <https://doi.org/10.1002/2015TC004109>
- Barry, T. L., Kelley, S. P., Reidel, S. P., Camp, V. E., Self, S., Jarboe, N. A., et al. (2013). Eruption chronology of the Columbia River Basalt Group. In *The Columbia River Flood Basalt Province* (Vol. 497, pp. 45–66). Geological Society of America. [https://doi.org/10.1130/2013.2497\(02\)](https://doi.org/10.1130/2013.2497(02))
- Berner, R. A., Lasaga, A. C., & Garrels, R. M. (1983). The carbonate-silicate geochemical cycle and its effect on atmospheric carbon dioxide over the past 100 million years. *American Journal of Science*, *283*(7), 641–683. <https://doi.org/10.2475/ajs.283.7.641>
- Bianchi, T. S., Cui, X., Blair, N. E., Burdige, D. J., Eglinton, T. I., & Galy, V. (2018). Centers of organic carbon burial and oxidation at the land-ocean interface. *Organic Geochemistry*, *115*, 138–155. <https://doi.org/10.1016/J.ORGEOCHEM.2017.09.008>
- Bindeman, I. N., Greber, N. D., Melnik, O. E., Artyomova, A. S., Utkin, I. S., Karlstrom, L., & Colón, D. P. (2020). Pervasive hydrothermal events associated with large igneous provinces documented by the Columbia River Basaltic Province. *Scientific Reports*, *10*(11), 1–9. <https://doi.org/10.1038/s41598-020-67226-9>
- Bretschneider, L., Hathorne, E. C., Huang, H., Lübbers, J., Kochhann, K. G. D., Holbourn, A., et al. (2021). Provenance and weathering of clays delivered to the Bay of Bengal during the Middle Miocene: Linkages to tectonics and monsoonal climate. *Paleoceanography and Paleoclimatology*, *36*(2), e2020PA003917. <https://doi.org/10.1029/2020PA003917>
- Browning, T. J., Stone, K., Bouman, H. A., Mather, T. A., Pyle, D. M., Moore, C. M., & Martinez-Vicente, V. (2015). Volcanic ash supply to the surface ocean – Remote sensing of biological responses and their wider biogeochemical significance. *Frontiers in Marine Science*, *2*, 14. <https://doi.org/10.3389/fmars.2015.00014>
- Brune, S., Williams, S. E., & Müller, R. D. (2017). Potential links between continental rifting, CO₂ degassing and climate change through time. *Nature Geoscience*, *10*(12), 941–946. <https://doi.org/10.1038/s41561-017-0003-6>
- Burdige, D. J. (2007). Preservation of organic matter in marine sediments: Controls, mechanisms, and an imbalance in sediment organic carbon budgets? *Chemical Reviews*, *107*(2), 467–485. <https://doi.org/10.1021/cr050347q>
- Burls, N. J., Bradshaw, C. D., De Boer, A. M., Herold, N., Huber, M., Pound, M., et al. (2021). Simulating Miocene warmth: Insights from an Opportunistic Multi-Model Ensemble (MioMIP1). *Paleoceanography and Paleoclimatology*, *36*(5), e2020PA004054. <https://doi.org/10.1029/2020PA004054>
- Caves Rugenstein, J. K., Ibarra, D. E., & von Blanckenburg, F. (2019). Neogene cooling driven by land surface reactivity rather than increased weathering fluxes. *Nature*, *571*(7763), 99–102. <https://doi.org/10.1038/s41586-019-1332-y>
- Clift, P. D., & Jonell, T. N. (2021). Himalayan-Tibetan Erosion is not the cause of Neogene global cooling. *Geophysical Research Letters*, *48*(8), e2020GL087742. <https://doi.org/10.1029/2020GL087742>
- Dal Corso, J., Mills, B. J. W., Chu, D., Newton, R. J., Mather, T. A., Shu, W., et al. (2020). Permo–Triassic boundary carbon and mercury cycling linked to terrestrial ecosystem collapse. *Nature Communications*, *11*(1), 1–9. <https://doi.org/10.1038/s41467-020-16725-4>
- Danišík, M., Ponomareva, V., Portnyagin, M., Popov, S., Zastrozhnov, A., Kirkland, C. L., et al. (2021). Gigantic eruption of a Carpathian volcano marks the largest Miocene transgression of Eastern Paratethys. *Earth and Planetary Science Letters*, *563*, 116890. <https://doi.org/10.1016/j.epsl.2021.116890>
- De Leeuw, A., Bukowski, K., Krijgsman, W., & Kuiper, K. F. (2010). Age of the Badenian salinity crisis; Impact of Miocene climate variability on the circum-mediterranean region. *Geology*, *38*(8), 715–718. <https://doi.org/10.1130/G30982.1>
- Deines, P. (2002). The carbon isotope geochemistry of mantle xenoliths. *Earth-Science Reviews*, *58*(3–4), 247–278. [https://doi.org/10.1016/S0012-8252\(02\)00064-8](https://doi.org/10.1016/S0012-8252(02)00064-8)
- Dessert, C., Dupré, B., François, L. M., Schott, J., Gaillardet, J., Chakrapani, G., & Bajpai, S. (2001). Erosion of Deccan Traps determined by river geochemistry: Impact on the global climate and the 87Sr/86Sr ratio of seawater. *Earth and Planetary Science Letters*, *188*(3–4), 459–474. [https://doi.org/10.1016/S0012-821X\(01\)00317-X](https://doi.org/10.1016/S0012-821X(01)00317-X)
- Dessert, C., Dupré, B., Gaillardet, J., François, L. M., & Allègre, C. J. (2003). Basalt weathering laws and the impact of basalt weathering on the global carbon cycle. *Chemical Geology*, *202*(3–4), 257–273. <https://doi.org/10.1016/j.chemgeo.2002.10.001>

- Domeier, M., & Torsvik, T. H. (2019). Full-plate modelling in pre-Jurassic time. *Geological Magazine*, 156(2), 261–280. <https://doi.org/10.1017/S0016756817001005>
- Donnadieu, Y., Godd  ris, Y., Pierrehumbert, R., Dromart, G., Jacob, R., & Fluteau, F. (2006). A GEOCLIM simulation of climatic and biogeochemical consequences of Pangea breakup. *Geochemistry, Geophysics, Geosystems*, 7(11). <https://doi.org/10.1029/2006GC001278>
- Ernst, R. E., Bond, D. P., Zhang, S. H., Buchan, K. L., Grasby, S. E., Youbi, N., et al. (2021). Large Igneous Province Record Through Time and Implications for Secular Environmental Changes and Geological Time-Scale Boundaries. In R. E. Ernst, A. J. Dickson, & A. Bekker (Eds.), *Large Igneous Provinces: A Driver of Global Environmental and Biotic Changes* (pp. 1–26). American Geophysical Union (AGU). <https://doi.org/10.1002/9781119507444.ch1>
- Flower, B. P., & Kennett, J. P. (1993). Relations between Monterey Formation deposition and Middle Miocene global cooling: Naples Beach section, California. *Geology*, 21(10), 877–888. [https://doi.org/10.1130/0091-7613\(1993\)021<0877:rmbfda>2.3.co;2](https://doi.org/10.1130/0091-7613(1993)021<0877:rmbfda>2.3.co;2)
- F  llmi, K. B., Badertscher, C., de Kaenel, E., Stille, P., John, C. M., Adatte, T., & Steinmann, P. (2005). *Phosphogenesis and organic-carbon preservation in the Miocene Monterey Formation at Naples Beach, California - The Monterey hypothesis revisited* (Vol. 117, p. 589). Bulletin of the Geological Society of America. GeoScienceWorld. <https://doi.org/10.1130/B25524.1>
- Frogner, P., Reynir G  slason, S., &   skarsson, N. (2001). Fertilizing potential of volcanic ash in ocean surface water. *Geology*, 29(6), 4872. [https://doi.org/10.1130/0091-7613\(2001\)029<0487:fpovai>2.0.co;2](https://doi.org/10.1130/0091-7613(2001)029<0487:fpovai>2.0.co;2)
- Gaillardet, J., Dupr  , B., Louvat, P., & All  gre, C. J. (1999). Global silicate weathering and CO₂ consumption rates deduced from the chemistry of large rivers. *Chemical Geology*, 159(1–4), 3–30. [https://doi.org/10.1016/S0009-2541\(99\)00031-5](https://doi.org/10.1016/S0009-2541(99)00031-5)
- Gasson, E., DeConto, R. M., Pollard, D., & Levy, R. H. (2016). Dynamic Antarctic ice sheet during the early to mid-Miocene. *Proceedings of the National Academy of Sciences of the United States of America*, 113(13), 3459–3464. <https://doi.org/10.1073/pnas.1516130113>
- Godd  ris, Y., Donnadieu, Y., Le Hir, G., Lefebvre, V., & Nardin, E. (2014). The role of palaeogeography in the Phanerozoic history of atmospheric CO₂ and climate. *Earth-Science Review* (Vol. 128, pp. 122–138). Elsevier. <https://doi.org/10.1016/j.earscirev.2013.11.004>
- Godd  ris, Y., Le Hir, G., Macouin, M., Donnadieu, Y., Hubert-Th  ou, L., Dera, G., et al. (2017). Paleogeographic forcing of the strontium isotopic cycle in the Neoproterozoic. *Gondwana Research*, 42, 151–162. <https://doi.org/10.1016/j.gr.2016.09.013>
- Goldner, A., Herold, N., & Huber, M. (2014). The challenge of simulating the warmth of the mid-Miocene climatic optimum in CESM1. *Climate of the Past*, 10(2), 523–536. <https://doi.org/10.5194/cp-10-523-2014>
- Gruber, N., Keeling, C. D., & Bates, N. R. (2002). Interannual variability in the North Atlantic Ocean carbon sink. *Science*, 298(5602), 2374–2378. <https://doi.org/10.1126/science.1077077>
- Hansen, J., Sato, M., Russell, G., & Kharecha, P. (2013). Climate sensitivity, sea level and atmospheric carbon dioxide. *Philosophical Transactions of the Royal Society A: Mathematical, Physical and Engineering Sciences*, 371(2001), 20120294.
- Hartmann, J., Jansen, N., D  rr, H. H., Kempe, S., & K  hler, P. (2009). Global CO₂-consumption by chemical weathering: What is the contribution of highly active weathering regions? *Global and Planetary Change*, 69(4), 185–194. <https://doi.org/10.1016/j.gloplacha.2009.07.007>
- Hartmann, J., Moosdorf, N., Lauerwald, R., Hinderer, M., & West, A. J. (2014). Global chemical weathering and associated p-release - The role of lithology, temperature and soil properties. *Chemical Geology*, 363, 145–163. <https://doi.org/10.1016/j.chemgeo.2013.10.025>
- Hay, W. W., Migdisov, A., Balukhovskiy, A. N., Wold, C. N., Fl  gel, S., & S  ding, E. (2006). Evaporites and the salinity of the ocean during the Phanerozoic: Implications for climate, ocean circulation and life. *Palaogeography, Palaeoclimatology, Palaeoecology*, 240(1–2), 3–46. <https://doi.org/10.1016/j.palaeo.2006.03.044>
- Haywood, A. M., Tindall, J. C., Dowsett, H. J., Dolan, A. M., Foley, K. M., Hunter, S. J., et al. (2020). The Pliocene Model Intercomparison Project Phase 2: Large-scale climate features and climate sensitivity. *Climate of the Past*, 16(6), 2095–2123. <https://doi.org/10.5194/CP-16-2095-2020>
- Hodell, D. A., & Woodruff, F. (1994). Variations in the strontium isotopic ratio of seawater during the Miocene: Stratigraphic and geochemical implications. *Paleoceanography*, 9(3), 405–426. <https://doi.org/10.1029/94PA00292>
- Huber, M., & Caballero, R. (2011). The early Eocene equable climate problem revisited. *Climate of the Past*, 7(2), 603–633. <https://doi.org/10.5194/CP-7-603-2011>
- IPCC. (2014). Climate Change 2014: Impacts, adaptation, and vulnerability. Part B: Regional aspects In Barros, V. R., et al. (Eds.), *Contribution of Working Group II to the Fifth Assessment Report of the Intergovernmental Panel on Climate Change*. Cambridge University Press.
- Ivanov, A. V., He, H., Yan, L., Ryabov, V. V., Shevko, A. Y., Palesskii, S. V., & Nikolaeva, I. V. (2013). Siberian Traps large igneous province: Evidence for two flood basalt pulses around the Permo-Triassic boundary and in the Middle Triassic, and contemporaneous granitic magmatism. *Earth-Science Reviews* (Vol. 122, pp. 58–76). Elsevier. <https://doi.org/10.1016/j.earscirev.2013.04.001>
- Jacob, R. L. (1997). *Low frequency variability in a simulated atmosphere-ocean system*. Dissertation. The University of Wisconsin - Madison.
- Jones, M. T., & Gislason, S. R. (2008). Rapid releases of metal salts and nutrients following the deposition of volcanic ash into aqueous environments. *Geochimica et Cosmochimica Acta*, 72(15), 3661–3680. <https://doi.org/10.1016/j.gca.2008.05.030>
- Karas, C., N  rnberg, D., Bahr, A., Groeneveld, J., Herrle, J. O., Tiedemann, R., & Demenocal, P. B. (2017). Pliocene oceanic seaways and global climate. *Scientific Reports*, 7(1), 1–8. <https://doi.org/10.1038/srep39842>
- Kasbohm, J., & Schoene, B. (2018). Rapid eruption of the Columbia River flood basalt and correlation with the mid-Miocene climate optimum. *Science Advances*, 4(9), 8223. <https://doi.org/10.1126/sciadv.aat8223>
- Kasbohm, J., Schoene, B., & Burgess, S. (2021). *Radiometric Constraints on the Timing, Tempo, and Effects of Large Igneous Province Emplacement* (pp. 27–82). American Geophysical Union (AGU). <https://doi.org/10.1002/9781119507444.ch2>
- K  rschner, W. M., Kva  ek, Z., & Dilcher, D. L. (2008). The impact of Miocene atmospheric carbon dioxide fluctuations on climate and the evolution of terrestrial ecosystems. *Proceedings of the National Academy of Sciences of the United States of America*, 105(2), 449–453. <https://doi.org/10.1073/pnas.0708588105>
- Laurent, D., de Kaenel, E., Spangenberg, J. E., & F  llmi, K. B. (2015). A sedimentological model of organic-matter preservation and phosphogenesis in the Miocene Monterey Formation at Haskells Beach, Goleta (central California). *Sedimentary Geology*, 326, 16–32. <https://doi.org/10.1016/j.sedgeo.2015.06.008>
- Lear, C. H., Mawbey, E. M., & Rosenthal, Y. (2010). Cenozoic benthic foraminiferal Mg/Ca and Li/Ca records: Toward unlocking temperatures and saturation states. *Paleoceanography*, 25(4). <https://doi.org/10.1029/2009pa001880>
- Lee, C.-T. A., Jiang, H., Ronay, E., Minisini, D., Stiles, J., & Neal, M. (2018). Volcanic ash as a driver of enhanced organic carbon burial in the Cretaceous. *Scientific Reports*, 8(1), 4197. <https://doi.org/10.1038/s41598-018-22576-3>
- Lee, J., Kim, S., Lee, J. I., Cho, H. G., Phillips, S. C., & Khim, B. K. (2020). Monsoon-influenced variation of clay mineral compositions and detrital Nd-Sr isotopes in the western Andaman Sea (IODP Site U1447) since the late Miocene. *Palaogeography, Palaeoclimatology, Palaeoecology*, 538, 109339. <https://doi.org/10.1016/j.palaeo.2019.109339>
- Lefebvre, V., Donnadieu, Y., Godd  ris, Y., Fluteau, F., & Hubert-Th  ou, L. (2013). Was the Antarctic glaciation delayed by a high degassing rate during the early Cenozoic? *Earth and Planetary Science Letters*, 371–372, 203–211. <https://doi.org/10.1016/j.epsl.2013.03.049>

- Lessios, H. A. (2015). Appearance of an early closure of the Isthmus of Panama is the product of biased inclusion of data in the metaanalysis. In *Proceedings of the National Academy of Sciences of the United States of America* (Vol. 112), E5765. National Academy of Sciences. <https://doi.org/10.1073/pnas.1514719112>
- Levy, R., Harwood, D., Florindo, F., Sangiorgi, F., Tripathi, R., von Eynatten, H., et al. (2016). Antarctic ice sheet sensitivity to atmospheric CO₂ variations in the early to mid-Miocene. *Proceedings of the National Academy of Sciences of the United States of America*, 113(13), 3453–3458. <https://doi.org/10.1073/pnas.1516030113>
- Li, G., & Elderfield, H. (2013). Evolution of carbon cycle over the past 100 million years. *Geochimica et Cosmochimica Acta*, 103, 11–25. <https://doi.org/10.1016/j.gca.2012.10.014>
- Li, G., Hartmann, J., Derry, L. A., West, A. J., You, C. F., Long, X., et al. (2016). Temperature dependence of basalt weathering. *Earth and Planetary Science Letters*, 443, 59–69. <https://doi.org/10.1016/j.epsl.2016.03.015>
- Longman, J., Gernon, T. M., Palmer, M. R., Jones, M. T., Stokke, E. W., & Svensen, H. H. (2021). Marine diagenesis of tephra aided the Paleocene-Eocene Thermal Maximum termination. *Earth and Planetary Science Letters*, 571, 117101. <https://doi.org/10.1016/j.epsl.2021.117101>
- Longman, J., Mills, B. J. W., Manners, H. R., Gernon, T. M., & Palmer, M. R. (2021). Volcanic nutrient supply initiated Late Ordovician climate change and extinctions. *Nature Geoscience*, 14, 924–929. <https://doi.org/10.1038/s41561-021-00855-5>
- Longman, J., Palmer, M. R., Gernon, T. M., & Manners, H. R. (2019). The role of tephra in enhancing organic carbon preservation in marine sediments. *Earth-Science Reviews*, 192, 480–490. <https://doi.org/10.1016/j.earscirev.2019.03.018>
- Lukács, R., Harangi, S., Guillong, M., Bachmann, O., Fodor, L., Buret, Y., et al. (2018). Early to Mid-Miocene syn-extensional massive silicic volcanism in the Pannonian Basin (East-Central Europe): Eruption chronology, correlation potential and geodynamic implications. *Earth-Science Reviews* (Vol. 179, pp. 1–19). Elsevier B.V. <https://doi.org/10.1016/j.earscirev.2018.02.005>
- Merdith, A. S., Williams, S. E., Brune, S., Collins, A. S., & Müller, R. D. (2019). Rift and plate boundary evolution across two supercontinent cycles. *Global and Planetary Change*, 173, 1–14. <https://doi.org/10.1016/j.gloplacha.2018.11.006>
- Mills, B., Daines, S. J., & Lenton, T. M. (2014). Changing tectonic controls on the long-term carbon cycle from Mesozoic to present. *Geochemistry, Geophysics, Geosystems*, 15(12), 4866–4884. <https://doi.org/10.1002/2014GC005530>
- Mills, B. J. W., Donnadieu, Y., & Goddérès, Y. (2021). Spatial continuous integration of Phanerozoic global biogeochemistry and climate. *Gondwana Research*, 100, 73–86. <https://doi.org/10.1016/j.gr.2021.02.011>
- Mills, B. J. W., Scotese, C. R., Walding, N. G., Shields, G. A., & Lenton, T. M. (2017). Elevated CO₂ degassing rates prevented the return of Snowball Earth during the Phanerozoic. *Nature Communications*, 8(1), 1–7. <https://doi.org/10.1038/s41467-017-01456-w>
- Montes, C., Cardona, A., Jaramillo, C., Pardo, A., Silva, J. C., Valencia, V., et al. (2015). Middle Miocene closure of the Central American Seaway. *Science*, 348(6231), 226–229. <https://doi.org/10.1126/science.aaa2815>
- O’Dea, A., Lessios, H. A., Coates, A. G., Eytan, R. I., Restrepo-Moreno, S. A., Cione, A. L., et al. (2016). Formation of the Isthmus of Panama. *Science Advances* (Vol. 2). American Association for the Advancement of Science. <https://doi.org/10.1126/sciadv.1600883>
- Panitz, S., Salzmann, U., Risebrobakken, B., De Schepper, S., Pound, M. J., Haywood, A. M., et al. (2018). Orbital, tectonic and oceanographic controls on Pliocene climate and atmospheric circulation in Arctic Norway. *Global and Planetary Change*, 161, 183–193. <https://doi.org/10.1016/j.gloplacha.2017.12.022>
- Peryt, T. M. (2006). The beginning, development and termination of the Middle Miocene Badenian salinity crisis in Central Paratethys. *Sedimentary Geology*, 188–189, 379–396. <https://doi.org/10.1016/j.sedgeo.2006.03.014>
- Pisciotta, K. A., & Garrison, R. E. (1981). *Lithofacies and depositional environments of the Monterey formation* (pp. 97–122).
- Rae, J. W. B., Zhang, Y. G., Liu, X., Foster, G. L., Stoll, H. M., & Whiteford, R. D. M. (2021). Atmospheric CO₂ over the Past 66 million years from marine archives. *Annual Review of Earth and Planetary Sciences*, 49(1), 609–641. <https://doi.org/10.1146/annurev-earth-082420-063026>
- Raymo, M. E., & Ruddiman, W. F. (1992). Tectonic forcing of late Cenozoic climate. *Nature* (Vol. 359, pp. 117–122). Nature Publishing Group. <https://doi.org/10.1038/359117a0>
- Reidel, S. P. (2015). Igneous rock associations 15. The Columbia River basalt group: A flood basalt province in the Pacific Northwest, USA. *Geoscience Canada*, 42(1), 151–168. <https://doi.org/10.12789/geocanj.2014.41.061>
- Reidel, S. P., Camp, V. E., Tolan, T. L., & Martin, B. S. (2013). *The Columbia River flood basalt province: Stratigraphy, areal extent, volume, and physical volcanology* (Vol. 497, pp. 1–43). Special Paper of the Geological Society of America. [https://doi.org/10.1130/2013.2497\(01\)](https://doi.org/10.1130/2013.2497(01))
- Scotese, C. R., Song, H., Mills, B. J. W., & van der Meer, D. G. (2021). Phanerozoic paleotemperatures: The earth’s changing climate during the last 540 million years. *Earth-Science Reviews*, 215, 103503. Elsevier B.V. <https://doi.org/10.1016/j.earscirev.2021.103503>
- Shields, G. A., & Mills, B. J. W. (2021). Evaporite weathering and deposition as a long-term climate forcing mechanism. *Geology*, 49(3), 299–303. <https://doi.org/10.1130/G48146.1>
- Sosdian, S. M., Babila, T. L., Greenop, R., Foster, G. L., & Lear, C. H. (2020). Ocean carbon storage across the middle Miocene: A new interpretation for the Monterey Event. *Nature Communications*, 11(1), 1–11. <https://doi.org/10.1038/s41467-019-13792-0>
- Steinthsordtir, M., Coxall, H. K., de Boer, A. M., Huber, M., Barbolini, N., Bradshaw, C. D., et al. (2020). The Miocene: The future of the past. *Paleoceanography and Paleoclimatology*, 36(4), e2020PA004037. <https://doi.org/10.1029/2020pa004037>
- Steinthsordtir, M., Jardine, P. E., & Rember, W. C. (2021). Near-future pCO₂ during the hot miocene climatic optimum. *Paleoceanography and Paleoclimatology*, 36(1), e2020PA003900. <https://doi.org/10.1029/2020PA003900>
- Svensen, H., Planke, S., Polozov, A. G., Schmidbauer, N., Corfu, F., Podladchikov, Y. Y., & Jamtveit, B. (2009). Siberian gas venting and the end-Permian environmental crisis. *Earth and Planetary Science Letters*, 277(3–4), 490–500. <https://doi.org/10.1016/j.epsl.2008.11.015>
- Tada, R., Zheng, H., & Clift, P. D. (2016). Evolution and variability of the Asian monsoon and its potential linkage with uplift of the Himalaya and Tibetan Plateau. *Progress in Earth and Planetary Science* (Vol. 3). Springer Berlin Heidelberg. <https://doi.org/10.1186/s40645-016-0080-y>
- Vance, D., Teagle, D. A. H., & Foster, G. L. (2009). Variable Quaternary chemical weathering fluxes and imbalances in marine geochemical budgets. *Nature*, 458(7237), 493–496. <https://doi.org/10.1038/nature07828>
- Westerhold, T., Marwan, N., Drury, A. J., Liebrand, D., Agnini, C., Anagnostou, E., et al. (2020). An astronomically dated record of Earth’s climate and its predictability over the last 66 million years. *Science*, 369(6509), 1383–1387. <https://doi.org/10.1126/SCIENCE.ABA6853>
- Zachos, J. C., Dickens, G. R., & Zeebe, R. E. (2008). An early Cenozoic perspective on greenhouse warming and carbon-cycle dynamics. *Nature*, 451(7176), 279–283. <https://doi.org/10.1038/nature06588>
- Zhu, J., Poulsen, C. J., & Tierney, J. E. (2019). Simulation of Eocene extreme warmth and high climate sensitivity through cloud feedbacks. *Science Advances*, 5(9), eaax1874. <https://doi.org/10.1126/SCIADV.AAX1874>